

Lithium–Sulfur Batteries

How to cite: *Angew. Chem. Int. Ed.* **2021**, *60*, 17547–17555

International Edition: doi.org/10.1002/anie.202103303

German Edition: doi.org/10.1002/ange.202103303

Ultralight Electrolyte for High-Energy Lithium–Sulfur Pouch Cells

Tao Liu, Huajun Li, Jinming Yue, Jingnan Feng, Minglei Mao, Xiangzhen Zhu, Yong-sheng Hu, Hong Li, Xuejie Huang, Liquan Chen, and Liumin Suo*

Abstract: The high weight fraction of the electrolyte in lithium–sulfur (Li–S) full cell is the primary reason its specific energy is much below expectations. Thus far, it is still a challenge to reduce the electrolyte volume of Li–S batteries owing to their high cathode porosity and electrolyte depletion from the Li metal anode. Herein, we propose an ultralight electrolyte (0.83 g mL^{-1}) by introducing a weakly-coordinating and Li-compatible monoether, which greatly reduces the weight fraction of electrolyte within the whole cell and also enables Li–S pouch cell functionality under lean-electrolyte conditions. Compared to Li–S batteries using conventional counterparts ($\approx 1.2 \text{ g mL}^{-1}$), the Li–S pouch cells equipped with our ultralight electrolyte could achieve an ultralow electrolyte weight/capacity ratio (E/C) of 2.2 g Ah^{-1} and realize a 19.2% improvement in specific energy (from 329.9 to 393.4 Wh kg^{-1}) under $E/S = 3.0 \mu\text{L mg}^{-1}$. Moreover, more than 20% improvement in specific energy could be achieved using our ultralight electrolyte at various E/S ratios.

Introduction

Lithium–sulfur (Li–S) batteries possess the advantages of high theoretical specific energy (2600 Wh kg^{-1}), natural abundance of sulfur, and cost-effectiveness and are thus regarded as one of the most promising post-lithium-ion batteries.^[1] Unfortunately, the accessible specific energy of Li–S batteries, at approximately $300\text{--}400 \text{ Wh kg}^{-1}$, is less than 15% of its theoretical value and far below expectations.^[2] The high “dead weight” of inactive components, particularly of the flooded electrolyte is the primary barrier for realizing high-energy Li–S batteries.^[3] Even at electrolyte/sulfur ratio (E/S) = $2 \mu\text{L mg}^{-1}$, the weight fraction of the electrolyte still

exceeds 48.5 wt.% of the whole cell, which is twice that of lithium-ion batteries (LIBs), at 22.2 wt.% (Figure 1a and Figure S1). Such high dead weight of the electrolyte at the cell level leads to a specific energy loss of approximately 50%. Thus, the specific energy of Li–S batteries can be significantly enhanced by reducing the weight fraction of electrolyte within the cell.^[4] For example, if the E/S is decreased from 5 to $3 \mu\text{L mg}^{-1}$, the estimated specific energy of the full cell could be increased by 39.2%, from 411 to 572 Wh kg^{-1} . Thus, the amount of electrolyte is considered to be the most critical factor to alter the specific energy of the Li–S full cell; reducing the weight fraction of electrolyte is therefore a practical and useful method to enhance the specific energy of Li–S cells.^[6]

Considerable efforts have been made to decrease the electrolyte volume of Li–S batteries, including reducing cathode porosity,^[5] employing suitable catalysts,^[6] and regulating reaction mechanisms.^[7] However, there is limited scope for further reducing the E/S in Li–S batteries owing to the unique nature of Li–S chemistry.^[8] First, a large amount of conductive carbon ($> 30 \text{ wt.}\%$) is necessary to overcome the insulating property of sulfur, which leads to high porosity ($> 70 \text{ vol.}\%$); therefore, an excess of electrolyte is required to fill the abundant void space.^[9] Second, the electrolyte not only provides ionic conduction but also supports the cathode “solid–liquid–solid” conversion, and its viscosity and ionic mobility are highly dependent on the polysulfide concentration.^[10] A limited amount of electrolyte with a high concentration of polysulfides significantly compromises Li-ion mobility, resulting in a pronounced degradation in the electrochemical performance of the cell. Third, owing to the high reactivity of lithium metal and the fragile solid electrolyte interphase (SEI), the SEI films undergo destruction and reconstruction during cycling, thus leading to continuous electrolyte depletion.^[17] Therefore, considering these undesirable factors, it is nearly impossible to further reduce the electrolyte volume of Li–S batteries to the LIBs level.^[11]

Most previous studies focused too heavily on the electrolyte volume, but neglected the electrolyte density, which is proportional to the electrolyte weight at a fixed electrolyte volume. However, the density of conventional electrolyte (1 M LiTFSI in DME/DOL (1:1) with 2 wt% LiNO_3) is approximately 1.2 g mL^{-1} , even close to that of ester electrolyte ($\approx 1.3 \text{ g mL}^{-1}$, 1 M LiPF_6 in EC/DMC 1:1).^[10a] If a low-density electrolyte is used instead of the conventional electrolyte, the electrolyte weight can be significantly lowered at the same E/S ratio. As shown in Figure 1b, assuming the electrolyte density is reduced from 1.2 to 0.8 g mL^{-1} under otherwise identical conditions, the cell-level specific energy

[*] Dr. T. Liu, H. Li, J. Yue, J. Feng, Dr. M. Mao, X. Zhu, Prof. Y.-s. Hu, Prof. H. Li, Prof. X. Huang, Prof. L. Chen, Prof. L. Suo
Beijing Advanced Innovation Center for Materials Genome Engineering, Key Laboratory for Renewable Energy, Beijing Key Laboratory for New Energy, Material and Devices, Beijing National Laboratory for Condensed Matter Physics, Institute of Physics, Chinese Academy of Science
Beijing, 100190 (China)
E-mail: suoliumin@iphy.ac.cn
Prof. L. Suo
Center of Materials Science and Optoelectronics Engineering, University of Chinese Academy of Sciences
Beijing, 100049 (China)
and
Yangtze River Delta Physics Research Center Co. Ltd
Liyang, 213300 (China)

Supporting information and the ORCID identification number(s) for the author(s) of this article can be found under:
<https://doi.org/10.1002/anie.202103303>.

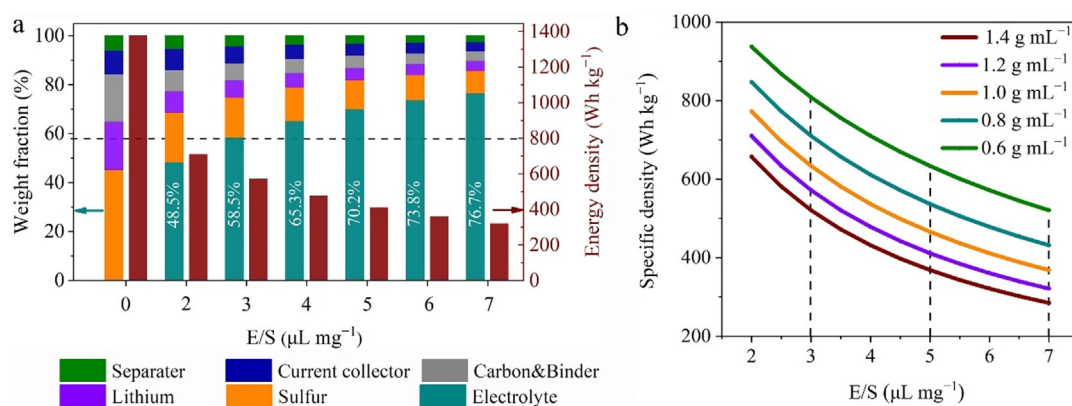


Figure 1. The influence of the electrolyte on the specific energy of Li-S full cell. a) Weight distribution and corresponding specific energy of Li-S full cell at varied E/S ratios. b) Relationship between the electrolyte density and the estimated specific energy of Li-S full cell (more details are provided in the Table S1).

would increase by 24.4 % at E/S = 3 μL mg⁻¹, 30.5 % at E/S = 5 μL mg⁻¹, and 34.3 % at E/S = 7 μL mg⁻¹.

Inspired by this, we propose a smart method to decrease the electrolyte density by introducing a novel Li-compatibility monoether. An ultralight electrolyte (0.4 m LiNO₃ + 0.2 m LiTFSI + DME/MPE (48:52, v/v)) with a density of 0.83 g mL⁻¹ was successfully demonstrated. A reduction of more than 30 % in the electrolyte weight per volume was realized using our ultralight electrolyte relative to the conventional electrolyte. Moreover, our ultralight electrolyte can enable Li-S battery functionality under lean-electrolyte conditions. The efficacy of the ultralight electrolyte was demonstrated on a Li-S pouch cell, which could deliver a specific energy of 393.4 Wh kg⁻¹, much higher than that delivered by conventional electrolyte (329.9 Wh kg⁻¹).

Results and Discussion

To identify the salts and their concentration-dependence electrolyte densities, we first evaluated the electrolyte densities of various different salts with varying concentrations. Other lithium salts (LiPF₆, LiBF₄, LiFSI, LiBOB, etc.) were excluded because of their chemical incompatibility with polysulfides or insolubility in ether solvents.^[12,13] Figure 2a shows that the electrolyte density increases with increasing salt concentration, and is also strongly associated with the type of anion. LiNO₃ showed the lowest density over the entire range of concentrations investigated, while the commonly used LiTFSI exhibited the highest density at the same concentration. Figure 2b shows the relationship between the ionic conductivities and the salt concentration within the range of 0.1–1.0 mol L⁻¹. The ionic conductivities of the electrolytes under the same concentration follow the order: LiTFSI > LiTf > LiBr > LiNO₃, because of the differences in the degree of dissociation.^[14] Additionally, the ionic conductivities of different electrolytes at similar densities follow the order: LiTFSI > LiNO₃ > LiTf > LiBr (Figure S2). Therefore, we selected the pair of salts LiNO₃-LiTFSI as the optimal bi-solute for our ultralight electrolyte. This selection not only provides acceptable ionic conductivity, but also contributes to

the stability of the Li anode due to its favorable SEI-forming properties (Figure S3).^[15]

In addition to salt, the electrolyte density is also highly dependent on the solvent. Solvent density is significantly correlated with molecular weight, polarity, structure, and functional groups.^[16] Figure 2c shows the density diagram of various solvents at 25 °C; the diagram is divided into four regions according to the density. Moving up the y-axis, it can be observed that the gas-liquid-solid phase diagrams correspond to the density < 0.6 g mL⁻¹, 0.6–1.8 g mL⁻¹, and

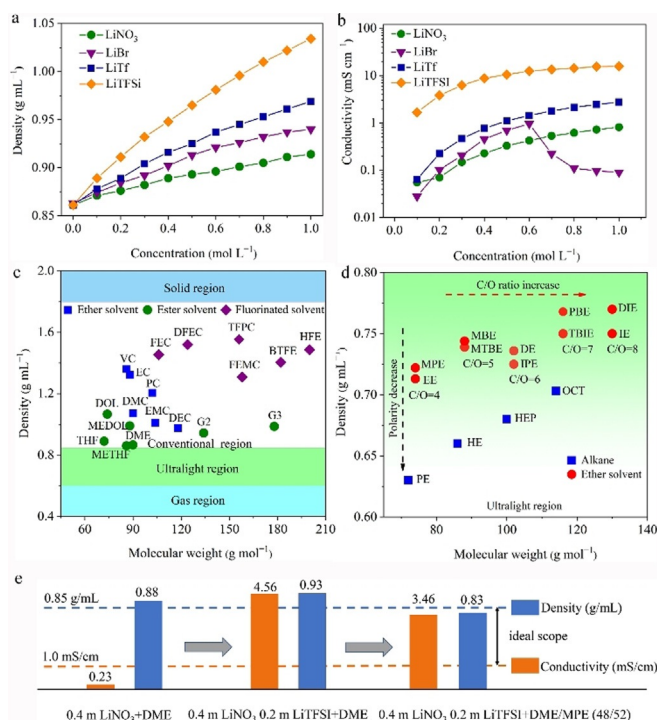


Figure 2. Selection and design of the ultralight electrolyte. a) Salts and the concentration-dependence of their electrolyte densities. b) Salts and the concentration-dependence of their ionic conductivities. c) Density diagram of common solvents. d) Solvent density in the ultralight region of (c). e) Schematic illustration of the optimization of the ultralight electrolyte.

$> 1.8 \text{ g mL}^{-1}$. In the density range less than 0.6 g mL^{-1} , the solvent molecules are typically nonpolar or possess small molecular sizes and usually gaseous at ambient temperature.^[17] Cooling or pressurizing these polar gases can lead to the formation of liquefied gas electrolytes, but will result in serious deterioration of the dynamic performance of Li–S. The liquid region can be further divided into two: the conventional region ($0.85\text{--}1.2 \text{ g mL}^{-1}$) and the ultralight region ($< 0.85 \text{ g mL}^{-1}$). It is obvious that the densities of conventional solvents, including ether, ester, and fluorinated solvents, are located in the conventional region. The ultralight region mainly consists of alkanes and monoethers, and their densities are mainly in the range of $0.6\text{--}0.8 \text{ g mL}^{-1}$. Alkanes were excluded from our investigations because salts are insoluble in them owing to the absence of nucleophilic sites in these molecules.^[18] Therefore, we focused on the monoethers, which possess a moderate dielectric constant that is beneficial for salt solubility and solvent mixing. Additionally, these monoethers possess high reductive stability because of the low oxygen content per volume and the electron-donating alkyl groups, displaying high compatibility with Li metal.^[19] As shown in Figure S4, methyl propyl ether (MPE) showed well-balanced stability and conductivity compared to EE, MBE, and MTBE under the same conditions. MPE was finally selected as the cosolvent to construct the ultralight electrolyte because of its low viscosity, moderate polarity, and inertness to lithium metal features. Figure 2e shows the design criteria for our ultralight electrolyte: 0.4 m LiNO_3 greatly enhances the interfacial stability of lithium metal, but does not provide satisfactory ionic conductivity (0.23 mScm^{-1}) due to its low degree of dissociation. Therefore, 0.2 M LiTFSI was added to increase the dissociation ratio of LiNO_3 and enhance the ionic conductivity. Finally, MPE was introduced as the ultralight solvent to afford the final composition (0.4 m LiNO_3 , 0.2 m LiTFSI , DME/MPE (48:52)), with a low density of 0.83 g mL^{-1} and high ionic conductivity of 3.46 mScm^{-1} .

Figure 3a summarizes the typical electrolytes that are available for Li–S batteries. Not even one electrolyte with a density below 1.0 g mL^{-1} is available; even in the electrolyte at 0.1 M concentration ($\approx 1.01 \text{ g mL}^{-1}$),^[20] is still $\approx 20 \text{ wt. \%}$ heavier than our ultralight electrolyte (ULE). Figure 3b further shows the advantages of the lightweight advantage of our ultralight electrolyte under varied E/S ratios. A much lower electrolyte/sulfur weight ratio (E_g/S_g) can be realized using our ultralight electrolyte at the same E/S ratio. Figure 3c shows that although the Li–Na alloy ($30\% \text{ Li} + 70\% \text{ Na}$) with a density of $\approx 0.84 \text{ g cm}^{-3}$ floats in electrolytes such as SIS and CE, the alloy sinks in our ultralight electrolyte, confirming its ultralow density. Furthermore, this can be further confirmed by their volumetric distinctions under the same mass condition (10 g); the filling volumes of SIS, CE, and ULE are 6.5 mL , 8.6 mL , and 12.1 mL , respectively (Figure S5). In other words, compared with SIS and CE, a reduction of 29.0 wt. \% and 45.5 wt. \% weight per volume was achieved by employing our ultralight electrolyte. This indicates that using the ultralight electrolyte is a universal and effective approach to alleviate the high weight fraction of the electrolytes in Li–S full cells.

Digital photos of the polysulfide dissolution experiment are shown in Figure S6. Our ultralight electrolyte contains more residual reactants, indicating the positive effect of suppressing polysulfide solubility owing to the weakly-solvating MPE. It should be noted that the appropriate polysulfide solubility of the ultralight electrolyte not only inhibits the shuttling effect, but also provides a suitable environment for the solid–liquid conversion reaction kinetics of the sulfur cathode.^[18] The ionic transportation of the ultralight electrolyte was further investigated. Figure 3d and e show the temperature-dependent ionic conductivities and viscosities of the three electrolytes. The ultralight electrolyte has a relatively high ionic conductivity of 3.46 mScm^{-1} at 25°C , which is lower than that of conventional electrolyte (12.14 mScm^{-1}) but much higher than that of SIS (0.97 mScm^{-1}). More importantly, our ultralight electrolyte exhibited a low activation energy of 2.29 kJ mol^{-1} , which indicated low energy barriers for ion transfer. The ultralight electrolyte also showed exceptionally low viscosity ($0.48\text{--}0.75 \text{ MPas}$), much lower than that of conventional ($1.73\text{--}3.11 \text{ MPas}$) and high concentration ($40\text{--}887 \text{ MPas}$) electrolytes, with minimal fluctuations in the wide temperature range from 0 to 50°C (Figure 3d); thereby displaying superior wettability for the porous separator and electrodes (Figure S7). This benefits the rate capability and the utilization of active materials.^[21] Raman spectroscopy was used to probe the electrolyte solvation structures. Two peaks at ≈ 820 and $\approx 850 \text{ cm}^{-1}$ were assigned to the uncoordinated oxide bonds of free DME.^[22] As shown in Figure 3f, the free DME peaks decreased with the introduction of the weakly coordinating MPE, indicating that Li^+ strongly prefers DME over MPE in the DME/MPE co-solvents. This behavior was further confirmed by the change in the ^{17}O NMR spectra under different conditions. The displacements of ethereal ^{17}O nuclei in DME were far greater than those in MPE when the salt was dissolved (Figure 3h). Contrary to the generalizations made regarding the solution structure, a peak at $\approx 745 \text{ cm}^{-1}$ derived from the coordination of TFSI^- to Li^+ usually appears in highly concentrated electrolytes,^[23] which reveals that TFSI^- is involved in the Li^+ solvation sheath even in a low-concentration salt owing to the addition of the weakly coordinating MPE (Figure 3g). This behavior can be explained by Zhang's work on a weakly-solvating electrolyte (WSE).^[24] When 0.4 m LiNO_3 is added to the $0.2 \text{ m LiTFSI} + \text{DME/MPE}$, the peak of $\text{Li}^+\text{-TFSI}^-$ disappears because the NO_3^- displaces the TFSI^- from the Li^+ solvation sheath due to the high donor number of NO_3^- . At the same time, a positive deviation of the NO_3^- peak, derived from the coordination of NO_3^- to Li^+ , was observed in the ultralight electrolyte (Figure S8a). It should be noted that TFSI^- was re-involved in the solvation sheath when the LiNO_3 was reduced to 0.2 m (Figure S8b); this indicated that LiNO_3 enhanced the dissociation of LiTFSI in weakly coordinating solvents due to its high donor number. Meanwhile, TFSI^- can be re-involved in the Li^+ solvation upon the consumption of NO_3^- during cycling,^[25] indicating that anion-derived solvation structures are normal in our ultralight electrolyte. This unique anion-derived solvation structure is not only conducive to sulfur utilization, but also

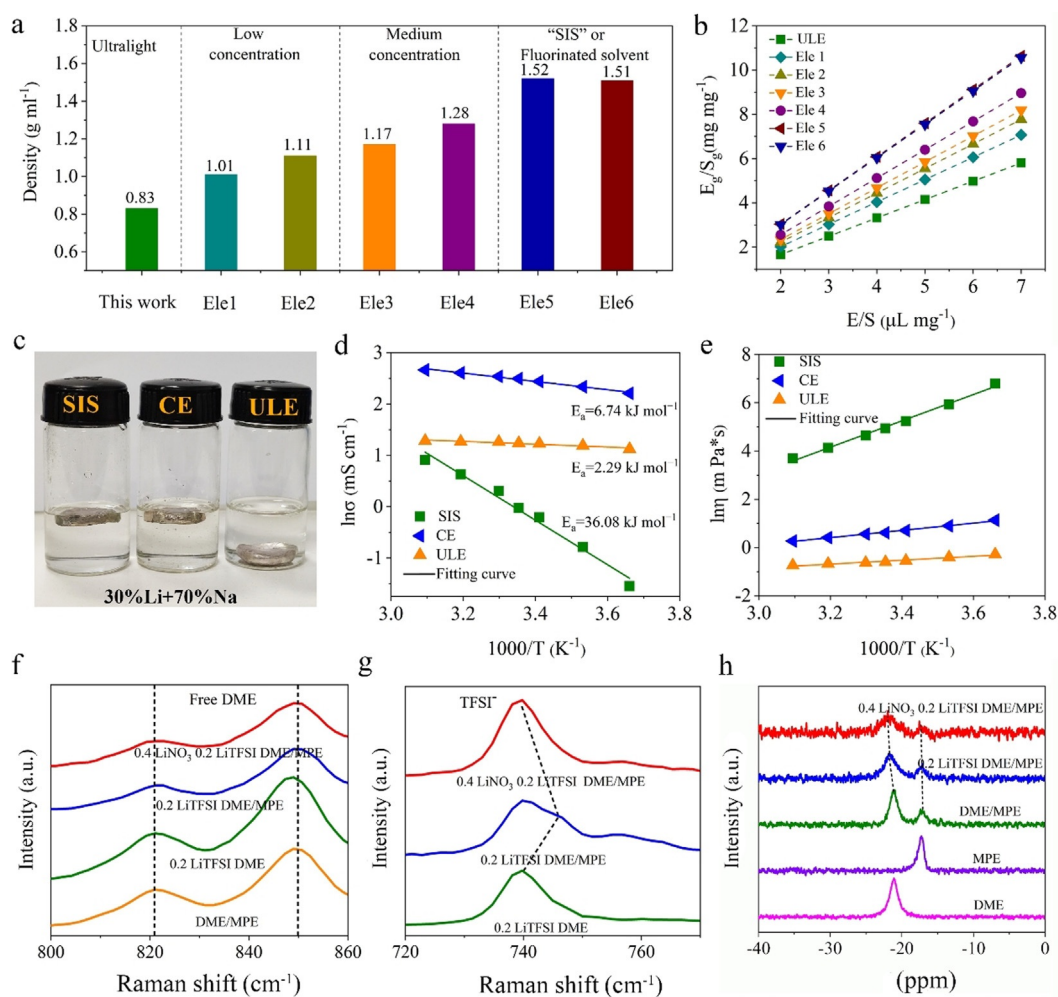


Figure 3. Physicochemical properties of the ultralight electrolyte (ULE). a) The densities of different electrolytes (Ele1: 0.1 M LiTFSI + 1 wt% LiNO₃ + DME/DOL (50/50),^[20] Ele2: 0.6 M LiTFSI + 0.4 M LiNO₃ + DME/DOL (50/50),^[5a] Ele3: 1.0 M LiTFSI + 2 wt% LiNO₃ + DME/DOL (50/50), denoted as CE,^[26] Ele4: 2.0 M LiTFSI + DOL,^[27] Ele5: 7 m LiTFSI + DME/DOL (50/50) denoted as SIS,^[28] Ele6: 1 M LiFSI + OFE/DME (95/5)^[29]). b) The electrolyte-weight/sulfur-weight (E_g/S_g) of different electrolytes under varied E/S ratios. c) Optical image of Li-Na alloy (30%Li + 70%Na) with a density of $\approx 0.84 \text{ g cm}^{-3}$ in three different electrolytes. d) Temperature-dependent ionic conductivities, and e) temperature-dependent viscosities. Raman spectra of different solutions in f) 800–860 cm^{-1} and g) 720–770 cm^{-1} . h) ^{17}O NMR spectra of the solvent in different mixtures.

suppresses ether solvent decomposition on the lithium surface.^[22]

Generally, the sulfur cathode has two distinct plateaus at 2.4 V and 2.1 V in the solid-liquid conversion process, whose capacity ratios can reflect the conversion efficiency from polysulfides to the reduction product Li₂S.^[30] As shown in Figure 4a, the Li-S batteries with the ultralight electrolyte displayed a higher Q_2/Q_1 ratio at different cycles, which indicated that the sulfur electrode exhibited superior reaction kinetics in the ultralight electrolyte. This was further confirmed by its rate capability and cycling stability. Li-S batteries with an ultralight electrolyte showed excellent rate capability (Figure 4b). The corresponding discharge capacities were 1072, 1018, 966, 846, and 714 mAh g^{-1} , at rates of 0.1, 0.2, 0.4, 0.8, and 1.0 C, respectively, and the capacity recovered to 1063 mAh g^{-1} after the rate shifted back to 0.1 C. As Figure 4c shows, Li-S batteries using the ultralight electrolyte displayed better cycling stability with a capacity retention of 71.5% after 200 cycles and a high average CE of

99.44%, which is much higher than that of the conventional electrolytes (46.9% and 98.06%, respectively). The Li-S batteries using ULE at a high current density of 1.0 C still exhibit excellent cycle stability (Figure S9). Moreover, the Li-S batteries with our ultralight electrolyte displayed much better performance than that with conventional electrolyte from -10 to 30°C (Figure S10). The morphology of the Li-metal anode before and after 200 cycles is shown in Figure 4d–f. Substantial cracking and a highly porous bulk structure on the Li surface were observed owing to the severe corrosion in the conventional electrolyte (Figure 4e). The black porous and “dead lithium” formation is greatly due to the continuous side reactions between the Li metal and the polysulfide-containing electrolyte. In contrast, the Li surface maintains larger Li particles with a dense and smooth surface in the ultralight electrolyte (Figure 4f), indicating excellent inhibition of the shuttling effect by our ultralight electrolyte. The EIS results after cycling agree well with the above results (Figure S11). To further demonstrate the efficacy of the

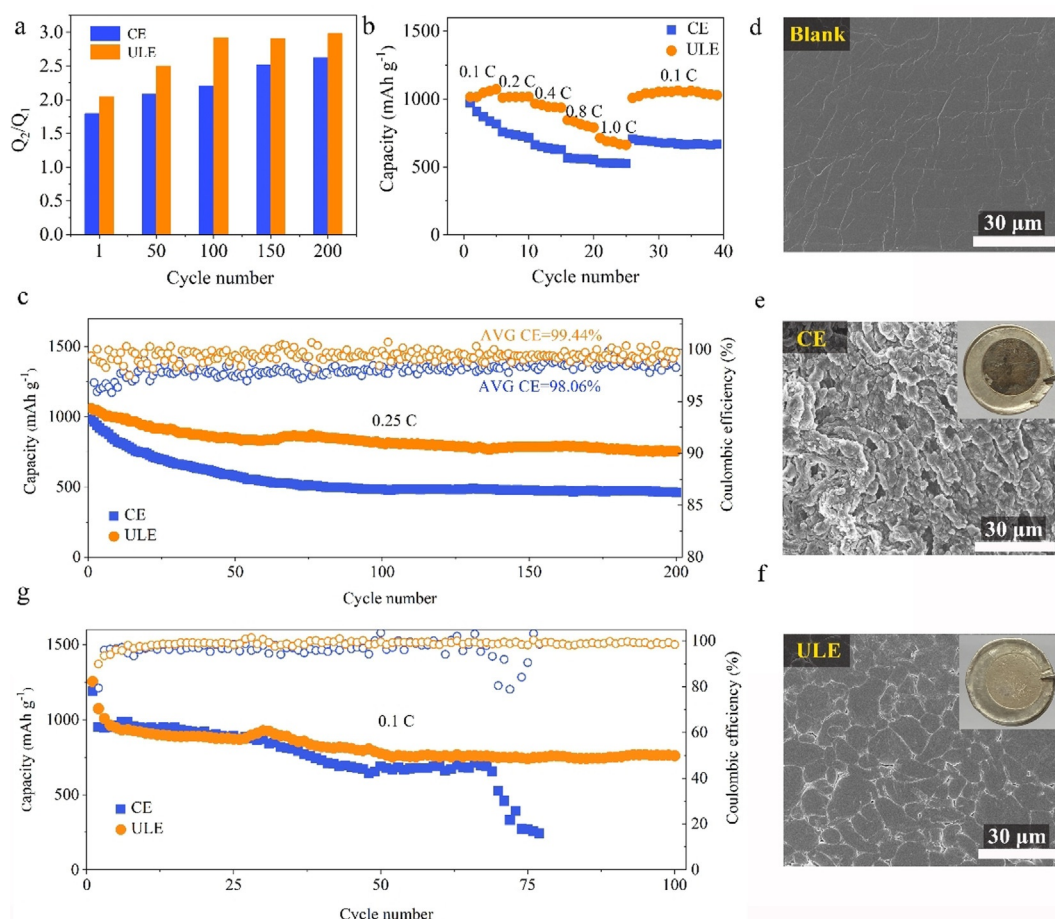


Figure 4. Electrochemical performance of ultralight electrolyte. a) The capacity ratio of the second discharge plateau to the first discharge plateau (Q_2/Q_1) at different cycles. b) The rate performance of Li–S batteries with different electrolytes. c) The cycling performance after activation of Li–S batteries ($\approx 1.2 \text{ mg cm}^{-2}$ loading) at 0.25 C. SEM images of the fresh lithium (d) and the cycled Li metal after 200 cycles in the conventional electrolyte (e) and ultralight electrolyte (f). g) The cycling stability of Li–S batteries at the sulfur loading of $\approx 3.9 \text{ mg cm}^{-2}$ at 0.1 C.

ultralight electrolyte, the cycling performance of Li–S batteries with a high sulfur loading was also investigated. To achieve stable cycle performance, fresh Li foil was pretreated ahead to reduce the side reactions between Li and electrolytes, especially the limited salt in the ultralight electrolyte. Mo_6S_8 was also introduced to the electrode because of its superior shuttle inhibition and electrocatalytic role in sulfur conversion.^[31] It should be noted that Mo_6S_8 can provide partially reversible capacity in the electrode.^[5a] The cells with the ultralight electrolyte showed a high capacity retention of 79% from the 3rd to the 100th cycle (Figure 4g). In contrast, the cells using the conventional electrolyte only survived for ≈ 75 cycles because of the capacity loss resulting from the severe shuttling effect, which can also be reflected by the severe corrosion of lithium metal (Figure S12). Moreover, the Li–S batteries using ultralight electrolyte could maintain more than 40 cycles under the lean-electrolyte condition of $E/S = 6.0 \mu\text{L mg}^{-1}$ (Figure S13). A small amount of $\text{Li}_2\text{S}/\text{Li}_2\text{S}_2$ was also observed on the cathode surface in the ultralight electrolyte, in sharp contrast to the conventional electrolyte, in which a thick $\text{Li}_2\text{S}/\text{Li}_2\text{S}_2$ clogged layer formed on the cathode surface (Figure S14,15). Uniform redistribution and

deposition of active materials in the electrode with ultralight electrolyte can be further confirmed by the EDS elemental maps (Figure S16). Low viscosity and abundant high donor number nitrate in the ultralight electrolyte are favorable for facilitating polysulfide transport and delaying electrode passivation, which agrees well with previous work by Kim.^[22] Nevertheless, the conventional electrolyte with high viscosity undesirably obstructs the dissolved polysulfides toward the inside of the cathode during cycling, resulting in the accumulation of deactivated $\text{Li}_2\text{S}/\text{Li}_2\text{S}_2$ and a significant degeneration in lithium-ion transport.^[32]

The behavior of Li electrodeposition was further investigated in an asymmetric Li–Cu cell configuration to evaluate the reversibility of the Li metal anode in the ultralight electrolyte. As shown in Figure 5a, the ultralight electrolyte shows a lower nucleation over potential and polarization than that of the conventional electrolyte, indicating its favorable facilitation of Li seeds. This may be attributed to the ultralow viscosity electrolyte enhancing Li-ion mobility and lowering of the Li^+ desolvation energy by the MPE addition.^[33] Moreover, the Li plating/stripping in the ultralight electrolyte exhibits high reversibility with a high coulombic efficiency of

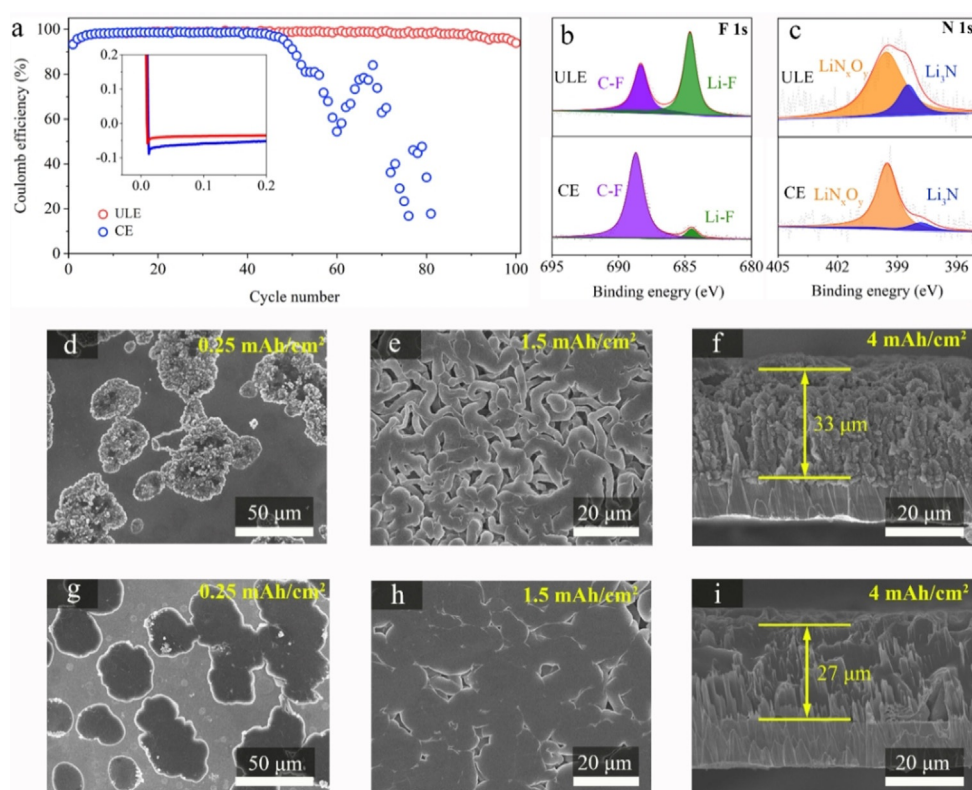


Figure 5. The behavior of Li electrodeposition in the ultralight electrolyte, a) The coulombic efficiency of Cu-Li cells cycled in different electrolytes, at a current density of 0.4 mA cm^{-2} and capacity of 1 mAh cm^{-2} . b) F 1s, c) N 1s XPS of lithium metal surface using different electrolytes after 2 cycles. SEM morphology of lithium deposited on the Cu with a current density of 0.4 mA cm^{-2} . A capacity of d) 0.25 mAh cm^{-2} , e) 1.5 mAh cm^{-2} lithium plating in conventional electrolyte. g) 0.25 mAh cm^{-2} , h) 1.5 mAh cm^{-2} lithium plating in ultralight electrolyte. The cross-section of 4.0 mAh cm^{-2} lithium plating in, f) conventional electrolyte, and i) ultralight electrolyte.

> 98% and longer cycling life > 90 cycles, compared to 50 cycles in the conventional electrolyte, which is much higher than 40 cycles of the low-concentration electrolyte (as shown in Figure S17). Increasing the deposition capacity to 4 mAh cm^{-2} , the Li-Cu cell using the ultralight electrolyte could still maintain more stable and higher CE compared to that with conventional ether-based electrolytes (Figure S18). The cycling efficiency of lithium metal is significantly dependent on the solid electrolyte interphase (SEI) and lithium deposition morphology. As shown in Figure 5b,c, X-ray photoelectron spectroscopy (XPS) reveals the existence of Li_3N , LiN_xO_y , and LiF, indicating the robust Li-N and LiF-dominant SEI formed on the surface of the cycled Li metal anode, which consequently facilitates ion transport and suppresses the parasitic reaction between the electrolyte and Li metal. Compared with the conventional electrolyte, a more pronounced LiF peak was found in the ultralight electrolyte resulting from the reduction of TFSI⁻ on the lithium surface. This was attributed to the fact that the solvent activity is greatly decreased by the addition of the weakly solvating MPE, and LiNO_3 and LiTFSI would be preferentially reduced on the lithium surface. Moreover, LiNO_3 can promote the decomposition of LiTFSI, forming LiF.^[24,25]

Figure 5d-i shows that the deposited lithium morphologies are highly dependent on the deposited capacities and the electrolytes. At a low deposition capacity of 0.25 mAh cm^{-2} in the conventional electrolyte, the Li deposition follows the island growth model, where irregular lithium randomly deposits to form isolated particles (Figure 5d). In contrast, the Li deposition in the ultralight electrolyte displayed dense and large grains (Figure 5g). With the increase in deposition capacity, the Cu substrate was gradually covered, and the lithium deposition in the conventional electrolyte evolved into a rod-like morphology (Figure 5e), accompanied by a high porosity. In contrast, Li metal in the ultralight electrolyte tended to deposit flatly and uniformly to finally grow into large grains (Figure 5g,h), resulting in dense Li deposition, which was also supported by the cross-sectional SEM of Li metal deposition at 4.0 mAh cm^{-2} (Figure 5i).

The Li deposition in our ultralight electrolyte was denser, with a thickness of only $27 \mu\text{m}$, much less than the $33 \mu\text{m}$ thickness in the conventional electrolyte (theoretical thickness: $20 \mu\text{m}$); the porosity of deposited Li reduced from 40% in the conventional electrolyte to 26% at the deposited capacity of 4.0 mAh cm^{-2} (Figure 5f). These results suggested that dense and uniform lithium deposition formed in the ultralight electrolyte, thereby resulting in prolonged cycling and higher coulombic efficiencies due to the reduced electrode/electrolyte contact area, uniform SEI growth, and inhibition of electrolyte consumption.

To further demonstrate the superiority of our ultralight electrolyte at the full cell level, a pouch cell ($\approx 65 \text{ mAh}$, single-layer) was assembled with an electrode area of 12 cm^2 , coupled with $50 \mu\text{m}$ Li foil (as shown in Figure S19). It is generally accepted that the soluble polysulfides would seriously compromise the ion mobility and mass transfer under lean-electrolyte conditions ($E/S < 3$), which would have a considerable influence on the kinetics of Li-S. Therefore, we evaluated the change in ionic conductivity and viscosity of the conventional (CE) and our ultralight electrolytes (ULE) before and after dissolving saturated polysulfides (Figure 6a,b). Compared with CE, ULE maintained a high ionic conductivity (from 3.73 to 4.74 mS cm^{-1}) and moderate

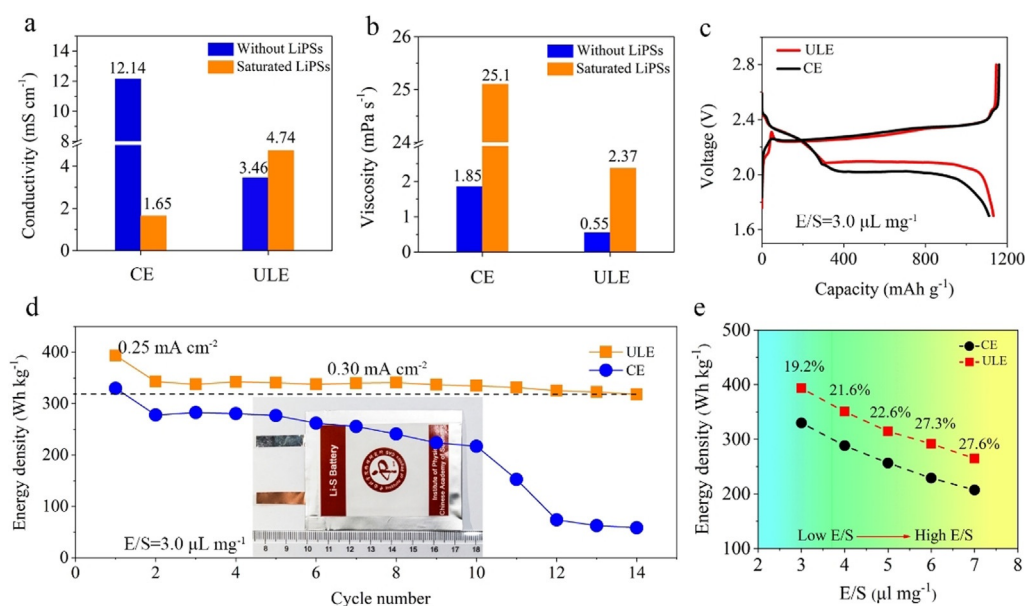


Figure 6. The Li–S pouch cells (≈ 65 mAh) with different electrolytes. The comparison of conductivities (a) and viscosities (b) of different electrolytes before and after dissolving saturated polysulfides. c) Initial charge-discharge curves of Li–S pouch cells at $E/S = 3.0 \mu\text{L mg}^{-1}$. d) The specific energy and cycling stability of pouch cells at $E/S = 3.0 \mu\text{L mg}^{-1}$. e) The improvement in specific energy of Li–S pouch cell by using the ultralight electrolyte at different E/S ratios.

viscosity (from 0.55 to 2.37 MPas⁻¹) under saturated polysulfide conditions, which is beneficial for accessing the soluble polysulfides throughout the porous electrode and forms effective ion channels between the cathode and anode; thereby, promoting sulfur redistribution and enhancing sulfur utilization. This was consistent with the electrochemical performance of Li–S pouch cells at $E/S = 3 \mu\text{L mg}^{-1}$, the discharge capacity (1111 mAh g^{-1}) of the Li–S cell with the conventional electrolyte was slightly lower than that of the ultralight electrolyte (1134 mAh g^{-1}), accompanied by a larger polarization (Figure 6c). The ultralight electrolyte in the pouch cell accounted for only 41.1 wt.%, lower than 49.6 wt.% of conventional electrolytes (Figure S20), thereby bringing out a 19.2% increment of specific energy from 329.9 to 393.4 Wh kg⁻¹ based on the single layer pouch cell with the single-sided coating on Al foil. It is expected that the value would further increase to 425.2 Wh kg⁻¹ if the cell is assembled into multiple-layer pouch cells due to the two-sided coating electrode. Moreover, paired with the pretreated lithium metal, the pouch cell with our ultralight electrolyte can run over 14 cycles with specific energy retention of more than 315 Wh kg⁻¹, much better than that with conventional electrolytes, which only survive 10 cycles with low specific energy < 250 Wh kg⁻¹ and rapid capacity fading (Figure 6d). In addition to $E/S = 3.0 \mu\text{L mg}^{-1}$, we further evaluated our ultralight electrolytes under various E/S ratios (Figure S21). By replacing the conventional electrolyte with our ultralight electrolyte, more than 20% increment in specific energy was achieved from extreme lean-electrolyte ($E/S = 3 \mu\text{L mg}^{-1}$) to normal lean-electrolyte ($E/S = 7 \mu\text{L mg}^{-1}$) on the pouch cell (Figure 6e). This indicated that our ultralight electrolyte has a universally positive effect on the increase in the specific energy independent of the E/S ratio. By a more intuitive

comparison with the previous work on Li–S batteries using the lean electrolyte (Figure S22), the parameter of electrolyte weight to the cell-capacity ratio, denoted as E/C (g Ah^{-1}) ratio in lithium-ion batteries is applied to quantify the electrolyte amount. Using our ultralight electrolyte, the E/C in the Li–S full cell was reduced to an ultralow $E/C = 2.2 \text{ g Ah}^{-1}$, less than half of that in previous reports under lean electrolyte conditions, and even lower than that of lithium-ion batteries (3.0 g Ah^{-1}). To the best of our knowledge, this low E/C represents a new level that is significant for Li–S cells to realize higher specific energy. Notably, our demonstrated Li–S pouch cell was only a handmade prototype without any other optimization. If coupled with further improvements to the cathode, with high sulfur loading and utilization, the specific energy is expected to increase further to surpass 500 Wh kg⁻¹.

Conclusion

We proposed a new class of ultralight electrolytes to tackle the high weight fraction of inactive electrolytes in Li–S full cells. It was demonstrated that an ultralight electrolyte with a density of 0.83 g mL^{-1} not only achieved 30% weight reduction per volume, as compared to the conventional electrolyte, but also exhibited excellent compatibility with lithium metal. Using our ultralight electrolyte in a pouch cell dramatically reduced the weight ratio of electrolyte and maintained high sulfur utilization under lean-electrolyte conditions, thus resulting in an ultralow electrolyte content of 2.2 g Ah^{-1} . The cell-level specific energy reached 393.4 Wh kg^{-1} at $E/S = 3 \mu\text{L mg}^{-1}$ at the sulfur loading of 4.8 mg cm^{-2} . Furthermore, when the E/S ratio changed from

$3 \mu\text{Lmg}^{-1}$ to $7 \mu\text{Lmg}^{-1}$, the energy densities of full cells increased by at least 20% with our ultralight electrolyte. This means that the employment of ultralight electrolytes is indeed a universal method to increase the specific energy of the Li-S full cell, independent of the E/S ratio and unaffected by the cathode and anode. We believe that our work provides a new and feasible strategy to improve the actual specific energy of Li-S batteries. In the future, with the discovery of more ultralight electrolytes, it is anticipated that the specific energy of Li-S batteries will increase further in the full cell-level specific energy.

Acknowledgements

This work is supported by the Center for Clean Energy. Tao Liu acknowledges China Postdoctoral Science Foundation (2019M660846).

Conflict of interest

The authors declare no conflict of interest.

Keywords: electrolytes · high specific energy · Li-compatible monoether · lithium-sulfur batteries · ultralight

- [1] a) J. Liu, Z. Bao, Y. Cui, E. J. Dufek, J. B. Goodenough, P. Khalifah, Q. Li, B. Y. Liaw, P. Liu, A. Manthiram, Y. S. Meng, V. R. Subramanian, M. F. Toney, V. V. Viswanathan, M. S. Whittingham, J. Xiao, W. Xu, J. Yang, X.-Q. Yang, J.-G. Zhang, *Nat. Energy* **2019**, *4*, 180–186; b) S. H. Chung, A. Manthiram, *Adv. Mater.* **2018**, *30*, 1705951; c) Y. Jin, K. Liu, J. Lang, X. Jiang, Z. Zheng, Q. Su, Z. Huang, Y. Long, C.-a. Wang, H. Wu, Y. Cui, *Joule* **2020**, *4*, 262–274.
- [2] C. Zhao, G. L. Xu, Z. Yu, L. Zhang, I. Hwang, Y. X. Mo, Y. Ren, L. Cheng, C. J. Sun, Y. Ren, X. Zuo, J. T. Li, S. G. Sun, K. Amine, T. Zhao, *Nat. Nanotechnol.* **2020**, *16*, 166–173.
- [3] A. Bhargava, J. He, A. Gupta, A. Manthiram, *Joule* **2020**, *4*, 285–291.
- [4] S.-H. Chung, C.-H. Chang, A. Manthiram, *Adv. Funct. Mater.* **2018**, *28*, 1801188.
- [5] a) W. Xue, Z. Shi, L. Suo, C. Wang, Z. Wang, H. Wang, K. P. So, A. Maurano, D. Yu, Y. Chen, L. Qie, Z. Zhu, G. Xu, J. Kong, J. Li, *Nat. Energy* **2019**, *4*, 374–382; b) Q. Pang, X. Liang, C. Y. Kwok, J. Kulisch, L. F. Nazar, *Adv. Energy Mater.* **2017**, *7*, 1601630.
- [6] a) Y. Yang, Y. Zhong, Q. Shi, Z. Wang, K. Sun, H. Wang, *Angew. Chem. Int. Ed.* **2018**, *57*, 15549–15552; *Angew. Chem.* **2018**, *130*, 15775–15778; b) Y. Song, W. Cai, L. Kong, J. Cai, Q. Zhang, J. Sun, *Adv. Energy Mater.* **2020**, *10*, 1901075; c) L. Peng, Z. Wei, C. Wan, J. Li, Z. Chen, D. Zhu, D. Baumann, H. Liu, C. S. Allen, X. Xu, A. I. Kirkland, I. Shakir, Z. Almutairi, S. Tolbert, B. Dunn, Y. Huang, P. Sautet, X. Duan, *Nat. Catal.* **2020**, *3*, 762–770.
- [7] a) C. Luo, E. Hu, K. J. Gaskell, X. Fan, T. Gao, C. Cui, S. Ghose, X. Q. Yang, C. Wang, *Proc. Natl. Acad. Sci. USA* **2020**, *117*, 14712–14720; b) Q. Pang, A. Shyamsunder, B. Narayanan, C. Y. Kwok, L. A. Curtiss, L. F. Nazar, *Nat. Energy* **2018**, *3*, 783–791; c) G. Zhang, H. J. Peng, C. Z. Zhao, X. Chen, L. D. Zhao, P. Li, J. Q. Huang, Q. Zhang, *Angew. Chem. Int. Ed.* **2018**, *57*, 16732–16736; *Angew. Chem.* **2018**, *130*, 16974–16978.
- [8] M. Zhao, B. Q. Li, H. J. Peng, H. Yuan, J. Y. Wei, J. Q. Huang, *Angew. Chem. Int. Ed.* **2020**, *59*, 12636–12652; *Angew. Chem.* **2020**, *132*, 12736–12753.
- [9] N. Kang, Y. Lin, L. Yang, D. Lu, J. Xiao, Y. Qi, M. Cai, *Nat. Commun.* **2019**, *10*, 4597.
- [10] a) S. Dörfler, H. Althues, P. Härtel, T. Abendroth, B. Schumm, S. Kaskel, *Joule* **2020**, *4*, 539–554; b) L. Cheng, L. A. Curtiss, K. R. Zavadil, A. A. Gewirth, Y. Shao, K. G. Gallagher, *ACS Energy Lett.* **2016**, *1*, 503–509.
- [11] L. Shi, S.-M. Bak, Z. Shadik, C. Wang, C. Niu, P. Northrup, H. Lee, A. Y. Baranovskiy, C. S. Anderson, J. Qin, S. Feng, X. Ren, D. Liu, X.-Q. Yang, F. Gao, D. Lu, J. Xiao, J. Liu, *Energy Environ. Sci.* **2020**, *13*, 3620–3632.
- [12] G. G. Eshetu, X. Judez, C. Li, M. Martinez-Ibanez, I. Gracia, O. Bondarchuk, J. Carrasco, L. M. Rodriguez-Martinez, H. Zhang, M. Armand, *J. Am. Chem. Soc.* **2018**, *140*, 9921–9933.
- [13] C. C. Su, M. He, R. Amine, Z. Chen, K. Amine, *Angew. Chem. Int. Ed.* **2018**, *57*, 12033–12036; *Angew. Chem.* **2018**, *130*, 12209–12212.
- [14] H. Chu, H. Noh, Y. J. Kim, S. Yuk, J. H. Lee, J. Lee, H. Kwack, Y. Kim, D. K. Yang, H. T. Kim, *Nat. Commun.* **2019**, *10*, 188.
- [15] a) W. Li, H. Yao, K. Yan, G. Zheng, Z. Liang, Y. M. Chiang, Y. Cui, *Nat. Commun.* **2015**, *6*, 7436; b) X. R. Chen, Y. X. Yao, C. Yan, R. Zhang, X. B. Cheng, Q. Zhang, *Angew. Chem. Int. Ed.* **2020**, *59*, 7743–7747; *Angew. Chem.* **2020**, *132*, 7817–7821; c) X. Liang, Z. Wen, Y. Liu, M. Wu, J. Jin, H. Zhang, X. Wu, *J. Power Sources* **2011**, *196*, 9839–9843.
- [16] W. George, Handbook of solvents, ChemTec Publishing, **2001**, pp. 42–43.
- [17] C. S. Rustomji, Y. Yang, T. K. Kim, J. Mac, Y. J. Kim, E. Caldwell, H. Chung, Y. S. Meng, *Science* **2017**, *356*, eaal4263.
- [18] A. Shyamsunder, W. Beichel, P. Klose, Q. Pang, H. Scherer, A. Hoffmann, G. K. Murphy, I. Krossing, L. F. Nazar, *Angew. Chem. Int. Ed.* **2017**, *56*, 6192–6197; *Angew. Chem.* **2017**, *129*, 6288–6293.
- [19] K. Sun, Q. Wu, X. Tong, H. Gan, *ACS Appl. Energy Mater.* **2018**, *1*, 2608–2618.
- [20] F. Wu, F. Chu, G. A. Ferrero, M. Sevilla, A. B. Fuertes, O. Borodin, Y. Yu, G. Yushin, *Nano Lett.* **2020**, *20*, 5391–5399.
- [21] a) S. Y. Lang, R. J. Xiao, L. Gu, Y. G. Guo, R. Wen, L. J. Wan, *J. Am. Chem. Soc.* **2018**, *140*, 8147–8155; b) W. Wang, Y. Wang, Y. Huang, C. Huang, Z. Yu, H. Zhang, A. Wang, K. Yuan, *J. Appl. Electrochem.* **2010**, *40*, 321–325.
- [22] H. Chu, J. Jung, H. Noh, S. Yuk, J. Lee, J. H. Lee, J. Baek, Y. Roh, H. Kwon, D. Choi, K. Sohn, Y. Kim, H. T. Kim, *Adv. Energy Mater.* **2020**, *10*, 2000493.
- [23] Y. Yamada, K. Furukawa, K. Sodeyama, K. Kikuchi, M. Yaegashi, Y. Tateyama, A. Yamada, *J. Am. Chem. Soc.* **2014**, *136*, 5039–5046.
- [24] Y. X. Yao, X. Chen, C. Yan, X. Q. Zhang, W. L. Cai, J. Q. Huang, Q. Zhang, *Angew. Chem. Int. Ed.* **2021**, *60*, 4090–4097; *Angew. Chem.* **2021**, *133*, 4136–4143.
- [25] J. Fu, X. Ji, J. Chen, L. Chen, X. Fan, D. Mu, C. Wang, *Angew. Chem. Int. Ed.* **2020**, *59*, 22194–22201; *Angew. Chem.* **2020**, *132*, 22378–22385.
- [26] T. Liu, S. Sun, J. Hao, W. Song, Q. Niu, X. Sun, Y. Wu, D. Song, J. Wu, *ACS Appl. Mater. Interfaces* **2019**, *11*, 15607–15615.
- [27] C. Qu, Y. Chen, X. Yang, H. Zhang, X. Li, H. Zhang, *Nano Energy* **2017**, *39*, 262–272.
- [28] L. Suo, Y. S. Hu, H. Li, M. Armand, L. Chen, *Nat. Commun.* **2013**, *4*, 1481.
- [29] J. Zheng, G. Ji, X. Fan, J. Chen, Q. Li, H. Wang, Y. Yang, K. C. DeMella, S. R. Raghavan, C. Wang, *Adv. Energy Mater.* **2019**, *9*, 1803774.
- [30] T. Liu, S. Sun, W. Song, X. Sun, Q. Niu, H. Liu, T. Ohsaka, J. Wu, *J. Mater. Chem. A* **2018**, *6*, 23486–23494.

- [31] K. Lu, Y. Liu, J. Chen, Z. Zhang, Y. Cheng, *ACS Nano* **2019**, *13*, 14540–14548.
- [32] a) W. Xue, D. Yu, L. Suo, C. Wang, Z. Wang, G. Xu, X. Xiao, M. Ge, M. Ko, Y. Chen, L. Qie, Z. Zhu, A. S. Helal, W.-K. Lee, J. Li, *Matter* **2019**, *1*, 1047–1060; b) H. J. Peng, J. Q. Huang, X. Y. Liu, X. B. Cheng, W. T. Xu, C. Z. Zhao, F. Wei, Q. Zhang, *J. Am. Chem. Soc.* **2017**, *139*, 8458–8466.
- [33] M. S. Park, S. B. Ma, D. J. Lee, D. Im, S. G. Doo, O. Yamamoto, *Sci. Rep.* **2014**, *4*, 3815.

Manuscript received: March 6, 2021
Revised manuscript received: May 11, 2021
Accepted manuscript online: May 24, 2021
Version of record online: June 23, 2021